scientific reports

Check for updates

OPEN

Synthesis, characterization, synergistic inhibition, and biological evaluation of novel Schiff base on 304 stainless steel in acid solution

Shimaa Hosny[1], Aliaa Abdelfatah[2] & Ghalia A. Gaber[3]✉

A novel Schiff base [4-(morpholin-4-yl) benzylidenyl]thiosemicarbazide (MBT) was created by reaction condensation. The molecules of the products were verified by IR, ^{1}HNMR, MS, and elemental techniques. The synergistic effect of KI with novel MBT on 304 stainless steel (SS) in acidic has been investigated experimentally and theoretically using DFT. The findings demonstrate that restriction efficacy on 304 SS improved with rising inhibitor concentrations, and this benefit was attributed to synergy when KI was injected. From EIS results, IE % increased with a higher concentration of MBT only and MBT + KI (from 100 to 600 ppm). MBT maximum IE % was 84.98%, at 600 ppm. MBT + KI, due to the I^- ions synergistic effect, showed an IE% of about 95.48%, at 600 ppm. The adsorptions of MBT and MBT + KI on the surfaces of 304 SS are strongly fitted Langmuir adsorption isotherms. Thermodynamic parameters (K_{ads}, ΔG^0_{ads}) were utilized. According to polarization findings, MBT behaves as a mixed-category antagonist. The Schiff base MBT was screened for its in vitro antimicrobial activities against some strains of bacteria and fungi. The result revealed that MBT proved to be an excellent candidate as a fungal agent being able to inhibit Aspergillus flavus.

One of the main industrial issues is corrosion, which causes damage to many petroleum installations, including reservoirs, distillation towers, and oil pipelines. Industries have implemented several techniques, including galvanizing, electroplating, and utilizing inhibitors, to reduce losses. However, due to its simplicity and affordability, using an inhibitor is thought to be the best method among them[1–5]. As corrosion inhibitors, a variety of inorganic and organic, those with aromatic rings, N, S, and O atoms, have been researched and used more effectively, more affordable, environmentally benign, and non-toxic[6–8]. The best approach to stop the corrosion of 304 SS and GS in acidic is to utilize specific morpholinobenzyldine compounds[9]. Due to the π-orbital with the surface, compounds have high inhibitive characteristics[10]. Many compounds of Schiff bases that have an azomethine bond function as potent corrosion inhibitors[11]. The effectiveness of a compound can occasionally be increased by including additional chemicals that work in synergism. Numerous studies on the synergistic effect have been conducted and are being reviewed. The order of Cl, Br, and I has been seen to increase the synergistic action of the halides. Iodide exhibits the largest synergistic impact due to its size and polarizability[12]. Many organic compounds' corrosion on mild steel was studied. The potency of the hydrazide derivatives as corrosion inhibitors in acidic has been thoroughly researched[9]. To determine whether it is possible to relate chemical structures to inhibitory effects, the researchers also looked into quantum chemistry[13]. Recent advancements in prevention and control center on finding new organic molecules by improving upon the existing ones. The anticancer efficacy of a few carbohydrazide derivatives with furan units was synthesized, characterized, and reported. However, due to the molecular architectures and the presence of heteroatoms, the molecules' capacity to prevent metal corrosion was further studied using theoretical principles such as density functional theory (DFT) techniques[14–19]. Therefore, we report herein the synthesis of a novel Schiff base, of [4-(morpholin-4-yl) benzylidenyl]thiosemicarbazide(MBT) by collection of 4-morpholinobenzaldehyde with thiosemicarbazide in ethanol. The synthesized Schiff base has

[1]Chemistry Department, Faculty of Science, New Valley University, El-Kharga 72511, Egypt. [2]Mining, Petroleum and Metallurgical Engineering Department, Faculty of Engineering, Cairo University, Cairo, Egypt. [3]Department of Chemistry, Faculty of Science (Girls), Al-Azhar University, Yousef Abbas Str., P.O. Box: 11754, Nasr City, Cairo, Egypt. ✉email: ghaliaasaid@azhar.edu.eg

been characterized based on their elemental analysis, FT-IR, ^{1}HNMR, and mass spectral data. The impact of Schiff base on the corrosion and synergist of it with KI for 304 stainless steel (SS) in 1 M HCl was studied by gravimetric method, potentiodynamic polarization, and electrochemical impedance spectroscopy (EIS) measurements. Furthermore, the in vitro antimicrobial synthesized Schiff base was also evaluated against some strains of bacteria and fungi. The results were compared with quantum chemical data.

Experimental details

Spectral studies

A Perkin-Elmer elemental analysis (240c) was used to evaluate the CHNS contents. The melting point of the synthesized Schiff base was determined using the Gallenkamp equipment. FTIR spectra were acquired on a Shimadzu spectrophotometer using a KBr pellet in the (4000–400 cm^{-1}) range. On a BRUKER 400 MHz, 1HNMR spectra in DMSO-d6 were acquired. Mass spectra were obtained using a (MS-5988 GC–MS) set at 70 eV. Thermogravimetric analyses were carried out on a Shimadzu DTG-60H in an inert environment at 10 °C/min.

Synthesis of MBT

A novel Schiff base, of [4-(morpholin-4-yl)benzylidenyl]thiosemi-carbazide (MBT) was synthesized by condensation of 4-morpholinobenzaldehyde (0.01 Mol dm^{-3}) with thiosemicarbazide (0.01 mol dm^{-3}) in 50 ml ethanol. The progress of the reaction was monitored by TLC. The synthetic route is outlined in (Fig. 1). The solid product formed was collected by filtration and recrystallized from ethanol as red crystals; yielding 85%; mp. 270 °C.

Yield: 85%; M.P. 270 oC. UV–Vis spectroscopy; the bands at λ_{max} (386, 445, 468, and 539 nm) are attributed to (π–π^*) transition of the aromatic ring, (n–π^*) transition of imine (C=N), (n–π^*) transition of the phenolic group and charge-transfer (CT), respectively.

Electrode assembly

The WE 304 stainless steel (SS) has compositions of 0.64% Si, 15% Cr, 5% Ni, 2% Mn, 0.02% S, 0.05% C, 0.043% P, and balance Fe. Uniform surfaces of 304 SS specimens were prepared with a grinding machine using emery paper of different grades (220, 400, 800, and 1000).

Corrosive medium

The acidic solution was prepared by the dilution of A.R grade 37% of HCl with deionized H_2O. The concentrations of Schiff base MBT were chosen as (100, 200, 400, and 600 ppm). By adding 0.1 M KI, the synergist of iodide ions was investigated.

Corrosion studies

Gravimetric method

The gravimetric approach is the simplest way to evaluate corrosion losses. The samples are first properly cleaned, after which they are polished with different grades of SiC, washed in ethanol, rinsed in distilled H_2O, and then allowed to dry. Following these stages, the specimens were precisely weighed before being submerged in 50 mL of 1 M HCl in both the presence and absence of various inhibitor doses (100, 200, 400, and 600 ppm). At a temperature of 25 °C, weight loss measurements were collected over 5 days. The specimens were removed from the test solution, completely cleaned of corrosion products, and then allowed to dry before being precisely reweighed[9]. Equation 1 [20] can be used to get the average weight reduction in grams:

$$\Delta W = W_i - W_f \tag{1}$$

where W_i = initial weight; W_f = final weight; ΔW = weight loss. The CR in mm/y is calculated in Eq. 2:

$$CR(mm/y) = \frac{\Delta W \times K}{A \times T \times D} \tag{2}$$

where: $K = 8.76 \times 10^4$, T = time in h, A = area in cm^2, ΔW = weight-loss in grams, and D = density in g/cm^3. The inhibition efficiency (IE) and surface coverage (θ) are determined by Eqs. (3) and (4), respectively.

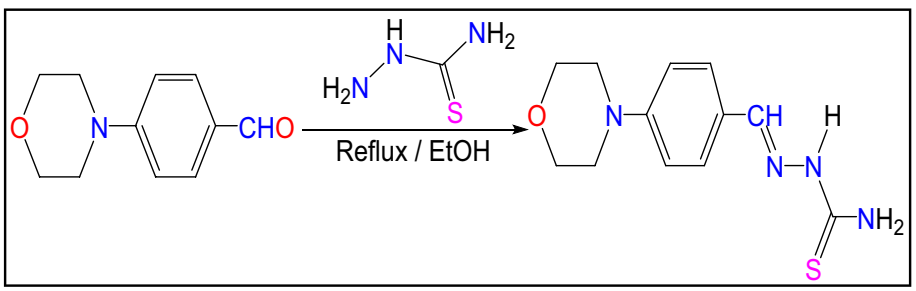

Figure 1. Synthesis of studied inhibitor (MBT).

$$\text{IE \%} = \frac{W_0 - W_{corr}}{W_0} \times 100 \quad (3)$$

where W_{corr} and W_o are the loss in the presence and absence of inhibitor, separately[11].

$$\text{Surface coverage } (\theta) = \frac{\text{IE}}{100} \quad (4)$$

PDP method
At a scan rate of 2 mV/s, polarization was produced in the electrode potential range of − 700 to + 700 $mV_{Ag/AgCl}$. To calculate current densities (I_{corr}), Tafel polarization analysis of anodic and cathodic curves was performed. Using Eq. 5, the inhibitive efficiency (IE%) was computed.

$$\text{IE \%} = 1 - \frac{CR_{inh}}{\text{CR}} \text{ x } 100 \quad (5)$$

where CR and CR_{inh} are the corrosion rates in the absence and presence of inhibitor, respectively[21].

EIS method
The impedance was done directly after keeping the electrode for 30 min until a steady-state open circuit potential (OCP) was reached. Corrosion inhibition measurements comprising EIS as well as PDP curves were completed in a three-electrode cell assembly using a VoltaMaster PGZ 301 potentiostat/galvanostat connected to a laptop. In this cell, the reference electrode, counter electrode, and working electrode are saturated calomel electrodes (SCE), platinum sheet electrode, and 304 SS, respectively. Because Schiff base compounds adsorbed to the 304 SS takes a certain amount of time, the 304 SS samples were dipped in 1 M HCl having diverse doses of Schiff base compounds for 30 min. After that, an almost stable state could be obtained for the open circuit potential (OCP). NOVA 1.11.2 software was used to fit the EIS curves to assume the impedance parameters such as electrolyte resistance (R_s), and charge transfer (R_{ct}).

Utilizing AC signals at OCP, the electrochemical impedance of 304 SS was performed in the frequency range of 100 kHz to 100 mHz with an amplitude of 10 mV peak-to-peak. Using charge transfer resistance values from Eq. 6[22], the IE% and θ were calculated.

$$IE\% = \theta \times 100 = 1 - \frac{Rct}{Rct_{inh}} \times 100 \quad (6)$$

where Rct and $Rct_{(inh)}$ are the charge transfer in the absence and presence of an inhibitor, respectively.

Computational details
The Schiff base ligand was optimized with the Gauss View 09 program B3LYP functional with 6-311++G basic set[23].

Biological activity
The prepared Schiff base ligand were screened against *Bacillus cereus (G + ve), E. coli (G−ve), Micrococcus luteus (G + ve), Pseudomonas aeruginosa (G−ve), Serratia marcescens (G−ve), Staphylococcus aureus (G + ve) bacteria and Aspergillus flavus, candida albicans, Fusarium oxysporum, Geotrichum candidum, Scopulariopsis brevicaulis and Trichophyton rubrum fungi*.

Results and discussion
Characterization of inhibitor
Analytical data
The data from elemental analysis of the newly synthesized MBT ligand agreed with the assumed molecular formulae, Table S1. This demonstrates the Schiff base ligand's purity.

^{1}H-NMR interpretation
The ^{1}H NMR of MBT in DMSO-d6 revealed the appearance of azomethine proton at δ: 7.70 ppm[24]. The NH proton signal was observed at δ: 8.10 ppm[25]. The signal at δ: 7.50 ppm for NH_2 proton. In addition, the presence of morpholine and aromatic system at δ: 3.30 and 6.90 ppm[25], respectively, indicates the purity of the prepared ligand (Fig. S1).

Infrared spectral of the Schiff base ligand (MBT)
The MBT ligand spectrum displayed absorption bands at 3174, 3340, and 758 cm-1, which are, respectively, attributed to (NH), (NH_2), and (C=S) groups. The imine signal of the ligand (C=N) at 1623 cm^{-1} reveals the production of the MBT ligand. (Fig. S2).

Mass spectral data
The MS of MBT revealed a molecular ion peak (*m/z*) at *m/z*: 266.05, which corresponds to the predicted molecular weight (Fig. 2). The MBT fragmentation route is distinguished by the presence of molecular ion peaks at

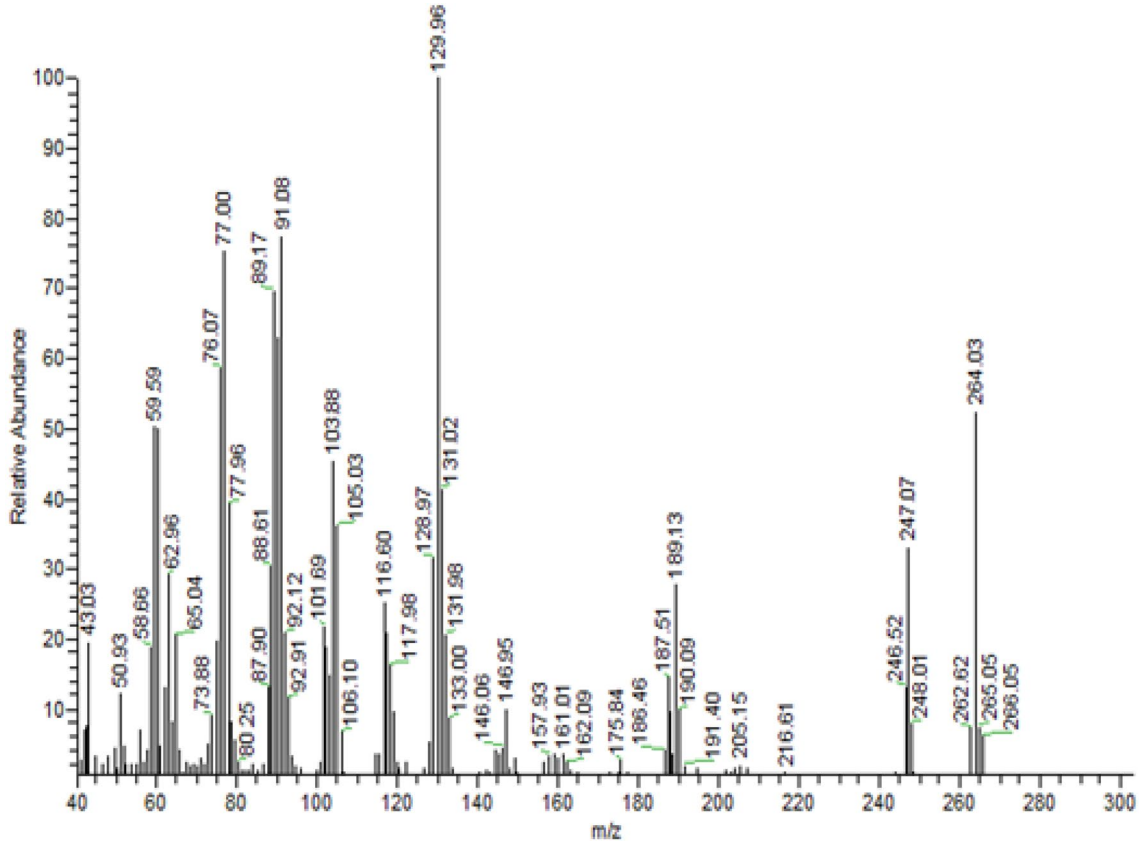

Figure 2. ESI–MS of the MBT Schiff base ligand.

m/z: 189.13 (27.78%) for $[M\text{-}C_{11}H_{13}ON_2]^+$, at *m/z*: 187.51 (14.14%) for $[M\text{-}C_6H_4]^+$ and base peak at *m/z*: 129.96 (100%), (Fig. 3).

Thermal analysis of MBT Schiff base ligand

The TG of MBT (Fig. S3) shows that completely decomposed with weight losses in two steps. The first step amounted to (calc. 38.5%, found 38.6%) at the temperature range between 116 and 428 °C, this can reveal the release of 2-methylene hydrazinecarbothioamide radical ($^{\cdot}C_2H_4N_3S$). The second mass loss is commensurate with the release of a 4-phenylmorpholine radical (calc. 61.3%, found 61.4%) at the temperature range between 428 and 691 °C (Fig. S4).

Corrosion studies

Gravimetric method

At 120 h, the weight loss of 304 SS in 1 M HCl at 25 °C with varying doses of inhibitor MBT and inhibitor + KI was assessed. Table 1 lists the corrosion rates, inhibition effectiveness, and surface coverage for 304 SS specimens. It is evident that as the inhibitor concentration increased from 100 to 600 ppm, the corrosion rate significantly decreased. Because the inhibitor molecules' surface is covered on the metal by adsorption. The synergistic impact of halide ions caused the corrosion rate to decrease with the addition of KI. The correlation of IE % against concentration of MBT and MBT + 0.1 M KI is represented in Fig. 4. As extra concentration causes the IE% to climb from 40.41 to 76.84% in the case of MBT alone, but increased from 79.01% to high of 91.79% in the presence of MBT + 0.1 M KI, it can be concluded that the addition of KI significantly strengthened the synergistic effectiveness of MBT inhibition. By conducting an intensified corrosion blockage of the active sites on the surface exposed to the media, the molecule adsorption will be gradually improved[26]. For all examined concentrations, it was discovered that the combination of inhibitor and KI has better inhibitory efficiency when compared to the values of inhibitor without KI. This work firmly demonstrates the part played by the Schiff base azomethine linkage (C=N), which actively contributes to the inhibitory mechanism.

Following the impact of concentration, this section will concentrate on immersion time because we are already aware of its influence on inhibitory performance. Studying its corrosion throughout a range of immersion times may be beneficial. Weight loss following varying immersion times in 1 M HCl with MBT and MBT + 0.1 M KI is shown in Fig. 5. These findings show that the IE % increases marginally throughout immersion time and peaks at 120 h, or 76.84% for the MBT inhibitor at an ideal concentration of 600 ppm. However, due to the significant reduction in the resistance of control, the efficiency of the examined compounds remains nearly consistent during a prolonged immersion time. The continued efficiency is a reflection of our chemical's capacity to create a solid, long-lasting protective layer on 304 SS surfaces surface in an acidic environment. The thickening of the

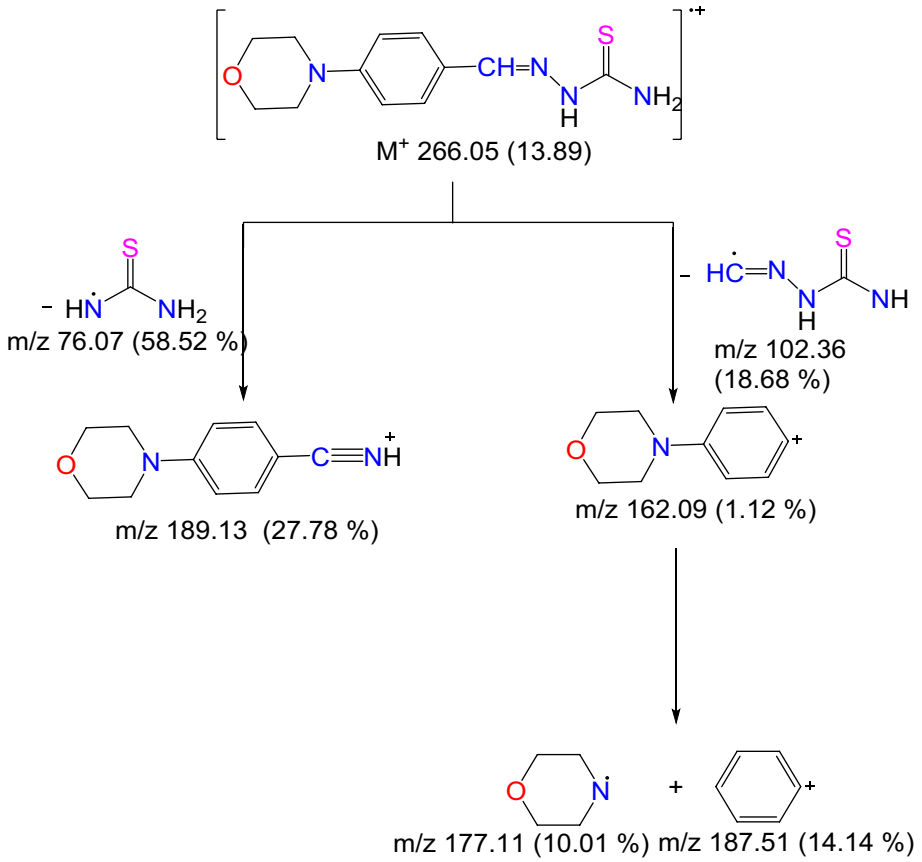

Figure 3. The fragmentation pathway of MBT.

Systems	Conc. (ppm)	WL (g)	C_R (mm/Y)	S.D	Θ	IE%
Blank 1M HCl	0.0	0.1460	3.3727	1.01×10^{-2}	–	–
1M HCl + 0.1M KI	0.0	0.1189	2.7467	5.01×10^{-2}	0.1856	18.56
MBT	100	0.0870	2.0098	1.11×10^{-1}	0.4041	40.41
	200	0.0602	1.3906	1.03×10^{-2}	0.5876	58.76
	400	0.0474	1.0950	1.53×10^{-3}	0.6753	67.53
	600	0.0338	0.7808	3.51×10^{-4}	0.7684	76.84
MBT + 0.1M KI	100	0.0190	0.4389	1.53×10^{-4}	0.7901	79.01
	200	0.0131	0.3026	1.69×10^{-2}	0.8555	85.55
	400	0.0110	0.2541	9.50×10^{-4}	0.8784	87.84
	600	0.0074	0.1709	2.09×10^{-3}	0.9179	91.79

Table 1. Corrosion rate, standard deviation (S.D), surface coverage, and inhibition efficiency for 304 SS corrosion in 1 M HCl in the absence and presence of MBT and MBT + KI at 25 °C.

film's formation is responsible for this outcome. According to earlier chemical research, the extent of dissolution is decreased[26,27]. Figure 6 displays the CR of 304 SS tracked in the MBT and MBT + KI systems at various concentrations. It can be demonstrated that the CR for systems MBT + KI is inhibitorier than without the addition of iodide, within the experimental error. We find that the synergistic efficiency of MBT inhibition has been substantially improved by the integration of KI.

PDP method

304 SS polarization curve in 1 M HCl with various concentrations of MBT with and without 0.1 M KI is depicted in Fig. 7. The potential corrosion (E_{corr}), Tafel slopes (β_a, β_c), current density (I_{corr}), rates of corrosion (CR), surface coverage (θ), S.D and efficiency (IE%) are presented in Table 2. The data demonstrate that adding concentrations of the Schiff base MBT reduces the values of I_{corr} and that this reduction is maintained when potassium iodide is also added. The adsorption of inhibitor molecules on the 304 SS by inhibiting the active sites on the steel

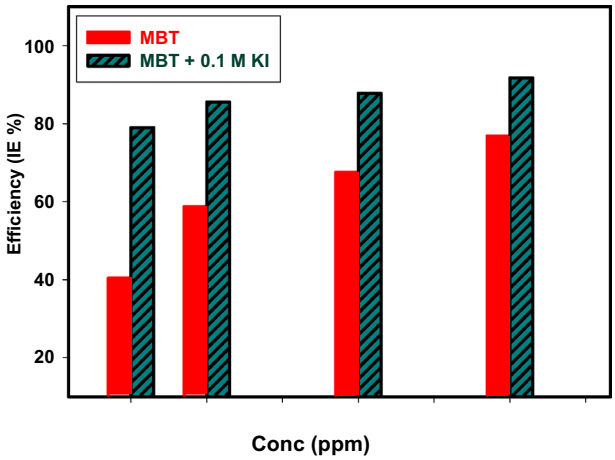

Figure 4. Correlation IE% of MBT and MBT + 0.1 M KI at 120 h.

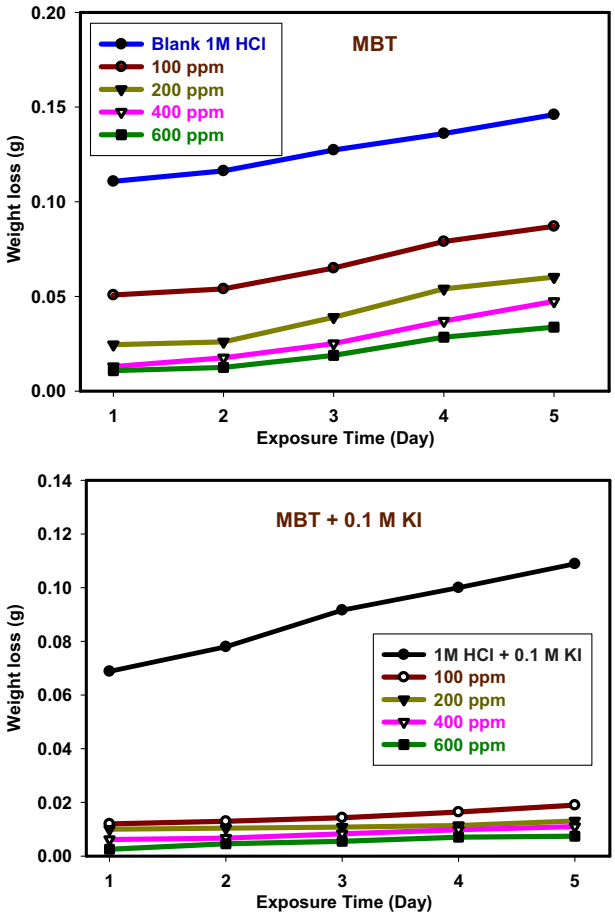

Figure 5. WL curve for 304 SS corrosion in 1 M HCl at various immersion times.

surface is the cause of the decrease in I_{corr}. The IE% readings in MBT only rise from 40.7 to 44.6% with increased concentration, but they grow from 62.3 to 90.6% in MBT with 0.1 M KI, indicating a greater surface coverage of the 304 SS. These results also demonstrate that MBT and KI work very well together to prevent corrosion of 304 SS. The anodic and cathodic reactions are therefore severely hindered. Although inhibitors can affect both cathodic and anodic processes, anodic reactions are primarily affected[12]. By adding more additives, the (E_{corr}) shifted to more positive values, but the shift, which was less than 85 mV, indicated that the effects of MBT and MBT + 0.1 M KI were mixed type[28,29].

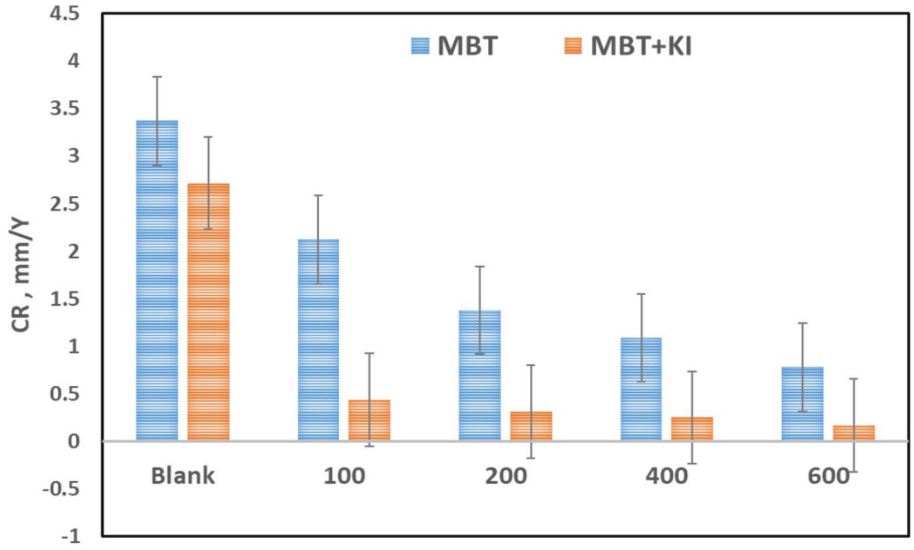

Figure 6. Error bar for comparing CR of 304 SS recorded in the system MBT and MBT + KI at different concentration.

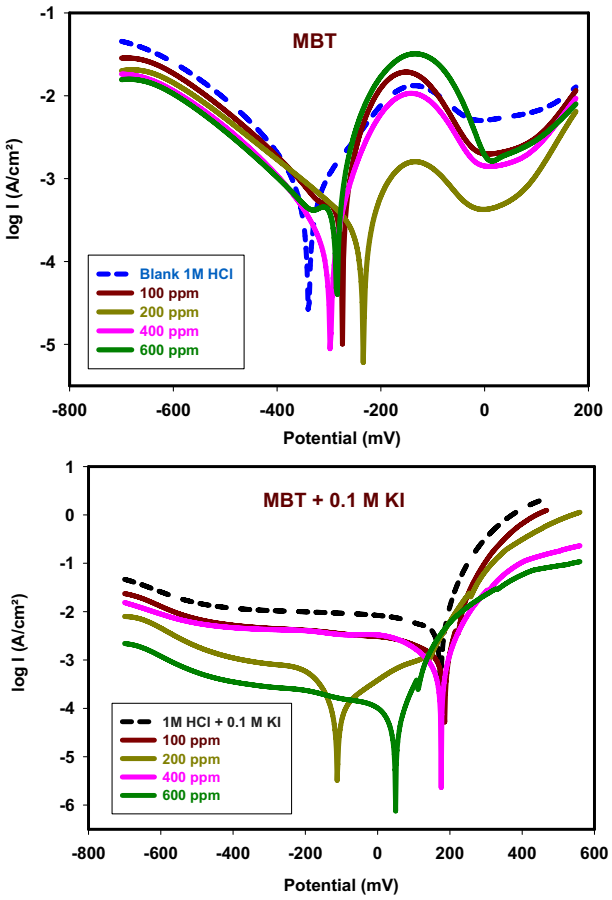

Figure 7. PDP curves for 304 SS in 1 M HCl in the absence and presence concentration of MBT and MBT + KI at 25 °C.

Systems	Conc. (ppm)	E_{corr} mV	I_{corr} mA/cm²	β_a mV/dec	β_c mV/dec	R_p ohm.cm²	C_R (mm/Y)	S.D	Θ	IE%
Blank 1 M HCl	0.0	− 344.9	0.3551	122.1	− 108.2	9.69	4.153	5.85×10^{-3}	–	–
1M HCl + 0.1M KI	0.0	145.3	0.2816	28.1	− 136.3	23.62	3.294	1.40×10^{-2}	0.206	20.6
MBT	100	− 282.2	0.2105	79.7	− 180.1	27.85	2.461	1.59×10^{-2}	0.407	40.7
	200	− 240.4	0.2049	59.0	− 138.5	46.05	2.396	6.08×10^{-3}	0.423	42.3
	400	− 304.6	0.2005	25.8	− 155.8	53.86	2.345	0.01×10^{-3}	0.435	43.5
	600	− 293.4	0.1967	48.9	− 402.3	54.08	2.300	2.08×10^{-2}	0.446	44.6
MBT + 0.1M KI	100	168.9	0.1339	91.8	− 412.9	87.19	1.567	7.00×10^{-3}	0.623	62.3
	200	− 116.7	0.0924	51.7	− 334.3	92.31	1.081	1.00×10^{-3}	0.739	73.9
	400	177.1	0.0647	192.7	− 102.0	211.80	0.756	1.00×10^{-3}	0.818	81.8
	600	43.1	0.0335	50.8	− 55.2	325.71	0.391	1.53×10^{-3}	0.906	90.6

Table 2. Corrosion parameters of PDP for 304 SS in 1M HCl in the absence and the presence concentration of MBT and MBT + KI at 25 °C.

EIS method

Figure 8 display the Nyquist and Bode plots of 304 SS immersed for 30 min in 1 M HCl free and containing various concentrations of MBT both with and without 0.1 M KI, respectively. The impedance response of 304 SS specimens differs noticeably when the KI with MBT is present and when it is not. The impedance graphs resemble semi-circular shapes. The semicircle's depressed nature is a feature of solid electrodes that exhibit frequency dispersion. This phenomenon is linked to a number of physical phenomena, such as surface roughness and solid

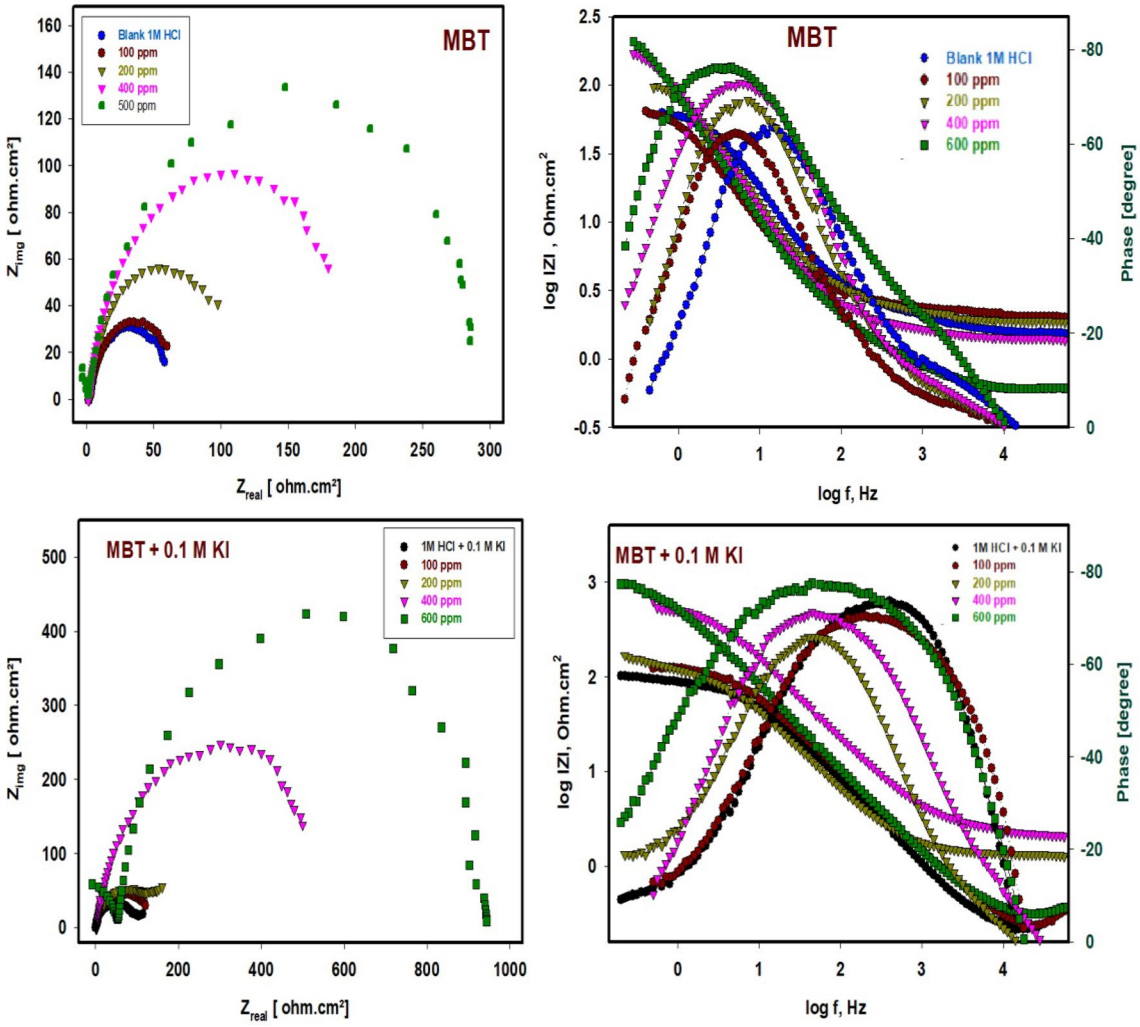

Figure 8. Nyquist and Bode plots for 304 SS in 1 M HCl in the absence and presence of concentration of MBT and MBT + KI at 25 °C.

electrode inhomogeneities. The Bode modulus showed three regions: a low frequency zone that suggests charge transfer resistance, a middle frequency region that indicates capacitive resistance, and a high frequency region that indicates solution resistance.

When the concentration of the inhibitors increases, the absolute Bode modulus value shifts to higher values in the low frequency zone, once more suggesting the formation of a protective film and, thus, efficient corrosion inhibition by greater inhibitor concentrations than lower ones. In every scenario, the phase angles are approaching 80^0. Pure electric models that might validate and make it possible under investigation can explain impedance behavior well[12]. Constant phase element (CPE) put into the circuit in place of C_{dl}, which produces a more accurate illustrated in Fig. 9 [30]. This reduces the effects caused by metal surface defects. Equation 7 can be used to express the impedance of CPE.

$$Z_{CPE} = \frac{1}{Y_0(j\omega)n} \tag{7}$$

where Y_0 is the magnitude of CPE, n is the phase shift, ω is the angular frequency, and j is the imaginary. CPE may be resistance, capacitance, and inductance depending upon the values of n[22]. EIS parameters and the efficiency of inhibition (IE%) are listed in Table 3. Values of CPE are reduced from 2.042 to 1.230 $mFcm^{-2}$ in the case of MBT only but, in the presence of MBT with 0.1 M KI reduced from 2.042 $mFcm^{-2}$ to reach 0.099 $mFcm^{-2}$, indicating that MBT is adsorbing on the surface of 304 SS in 1 M HCl.

The double layer that separates the charged metal surface from the solution and is thought of as an electrical capacitor may be used to explain this drop in C_{dl}[31]. Values of R_{ct} and the width of the capacitive loop are increased by MBT concentrations in the absence and existence of KI. When utilized inhibitors are present, R_{ct} values rise from 43.99 to 293 Ω cm^2 in the case of MBT alone, but rise from 43.99 to 973.78 Ω cm^2 in the case of MBT plus 0.1 M KI, increasing the width of the capacitive loop and raising IE%. The IE% rises from 52.55 to 84.98% in MBT alone, but from 68.80 to 95.48% in MBT with 0.1 M KI. According to the IE percentage data, KI significantly improves MBT's ability to reduce the rate of corrosion. These findings imply that the MBT works via adsorption at the interface and that I ions strengthen this adsorption.

The importance of phase angle measurement during the application of electrical impedance spectroscopy was studied. The depletion or phase angle is shown in Table 3. Electrical impedance, phase angle (strength of capacitive character), and dissipation factor were scanned between 100 and 10,000 Hz current frequency. In low-frequency regions in which the frequency is less than 100 Hz, the phase angles of impedance in different stages are similar. When the frequency is higher than 100 Hz, there is a significant difference between the phase angles of different impedances[32,33]. The absolute value of the phase angle increases constantly with more negative

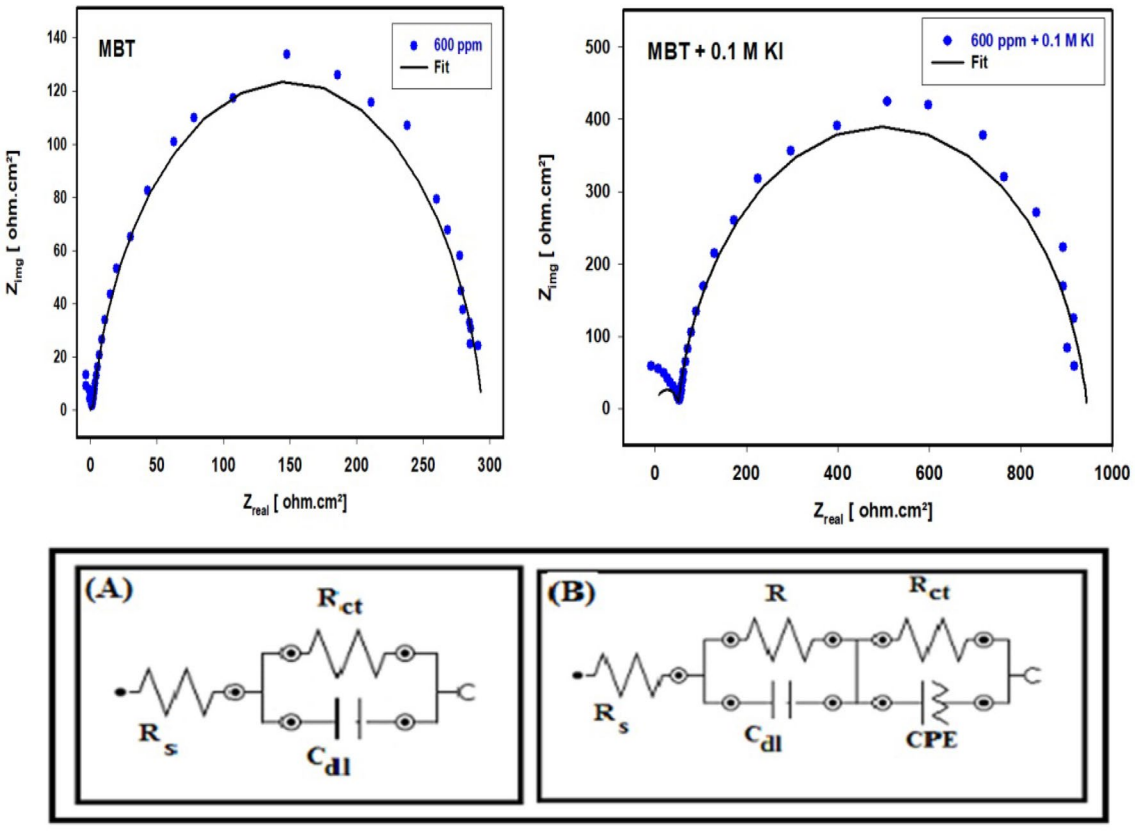

Figure 9. Comparison of fitted and investigational findings of 304 SS corrosion in the presence of MBT and MBT + KI and the equivalent circuit used (**A**, **B**).

Systems	Conc. (ppm)	R_s Ω.cm^2	R_{ct} Ω.cm^2	CPE mF/cm^2	n	R Ω.cm^2	C_{dl} mF/cm^2	χ^2	Depletion angle °	IE%
Blank 1M HCl	0.0	1.32	43.99	2.042	0.811			2.5	− 1.23	–
1M HCl + 0.1M KI	0.0	1.40	113.40	0.538	0.723			3.1	− 5.99	61.28
MBT	100	1.38	92.70	1.586	0.601	0.58	0.935	5.2	− 1.58	52.55
	200	1.73	135.30	1.481	0.770	0.85	0.873	7.0	− 4.88	67.48
	400	1.94	200.60	1.287	0.813	1.26	0.769	6.5	− 10.4	78.07
	600	1.00	293.00	1.230	0.893	1.84	0.725	7.1	− 19.8	84.98
MBT + 0.1M KI	100	2.32	141.00	0.280	0.900	0.89	0.165	3.2	− 9.09	68.80
	200	5.93	186.60	0.278	0.819	1.17	0.164	5.3	− 10.7	76.43
	400	2.41	601.90	0.225	0.743	3.78	0.133	3.2	− 13.0	92.69
	600	5.12	973.78	0.099	0.914	8.50	0.004	2.8	− 13.6	95.48

Table 3. Electrochemical impedance parameters for 304 SS in 1 M HCl in the absence and presence of a concentration of MBT and MBT + KI at 25 °C.

values leading to more protection occurring. The negative phase angle equals the voltage lags the current. With an RL circuit, current lags voltage, so, when we divide the voltage by the impedance of an RL circuit, we want the resulting current to have a negative (lagging) phase.

The phase angles are then given by Eq. 8

$$\phi = \tan^{-1}[(X_c - X_L)/R] \tag{8}$$

Note that if $X_L = 0$, meaning that there is no inductor in the circuit, then we arrive at the solution we obtained for the RC circuit. The enhancement in phase angle in the presence of MBT and MBT + KI molecules suggests that the adsorption of Schiff base compounds is what defines the capacitive routine of the surface of the metal/solution. More additives were adsorbed at the metal/electrolyte interface, generating an inhibitor-Fe complexing activity that was able to shield the metal surface from degradation and, as a result, increased a low corrosion rate. This is how the protective performance occurred[34].

The comparison of fitted and investigational findings of 304 SS corrosion with MBT and MBT + KI is illustrated in Fig. 9. Utilizing the equivalent circuit example assigned in Fig. 9A, B. The ideal equivalent circuit was utilized to obtain the impedance characteristics to mathematically interpret the electrochemical performance[35]. The EEC illustrated in Fig. 9A was utilized to normalize the results of the inhibitor-free (blank) system, whereas Fig. 9B provides the Equivalent circuit with MBT and MBT + KI.

Nyquist plots of solutions inhibited by Schiff base MBT and MBT + KI were best represented by the equivalent circuit shown in Fig. 9B. In both cases (MBT and MBT + KI), according to the phase angle, two time constants are observed. Based on the discussion of the EIS spectra, the equivalent circuit of two-time constants shown in Fig. 9B was used for the modeling of the electrochemical processes of MBT and MBT + KI. R_s represents the electrolyte resistance, CPE-R_{ct} represents the resistive–capacitive response of the first time constant, and C_{dl}-R represents the resistive–capacitive response of the second time constant. In the presence of MBT, from the Nyquist diagram, the apparent formation a time constant is observed between 1000 and 10,000 Hz whose capacitance decreases. From the Bode diagram in its impedance module format, in the high frequency region it is possible to observe the formation of the high frequency plateau starting at 1000 Hz; however, as time increases, its formation occurs at higher frequencies (> 10,000 Hz). In the region of intermediate frequency and low frequency, the apparent presence of a single linear relationship (log f–log |Z|) is observed, and it is not possible to define the low-frequency plateau. This suggests that the impedance modulus is greater than the recorded value.

In the presence of MBT + KI the maximum phase angles between 70° and 80° is very wide, suggesting at least two overlapping time constants. The first time constant shows an increase in its maximum phase angle and a displacement of its maximum at higher frequencies. The second time constant shows an increase in its maximum phase angle and a shift to lower frequencies. This behavior may be associated with the characteristics of the passive layer formed on MBT + KI; it is commonly accepted that the passive layer has a bilayer structure where the external part is porous (first time constant) and the internal part is compact and dense (second time constant) and therefore it presents the largest phase angle[32,33]. This result can reveal that there is more than one occurred electrochemical process, and the growth of more resistive MBT and MBT + KI layers adsorbed onto the SS surface, forming protected films.

The value of fitting was evaluated by chi error value (χ^2) listed in Table 3. The values of the EIS fitting parameters as CPE, n, and R_{ct} are listed in Table 3. As seen from Table 3, the increase of inhibitor concentrations is ascribed to increasing the surface coverage by MBT and MBT + KI. It can be noticed that R_{ct} and R values increased with increasing concentrations. The dose-dependent increase in R_{ct} indicates a rise in inhibition efficiency across the board. Adsorption of the tested compounds is likely responsible for restoring the metal's surface since the thickness of the adsorbed layer increases when inhibitor dosages are increased[36–38]. According to the above results, MBT and MBT + KI are suitable inhibitors for SS in HCl. Additionally, MBT in the presence of iodide exhibits a synergistic effect that enhances its inhibitory efficacy compared to MBT in the absence of iodide. There is a strong correlation between the findings from the polarization investigations and the impedance studies.

Adsorption isotherm and thermodynamic variables

To analyze the data, several adsorption isotherms, including Langmuir, Temkin, and Freundlich, were fitted. Using data from EIS measurements, the surface coverage and inhibitory efficiency are estimated and displayed in Table 3.

Langmuir adsorption isotherm

To scrutinize the adsorption process of inhibitors, the surface coverage (θ) was graphically determined from the EIS method through a suitable fitting of adsorption isotherm. The best relation was obtained from the Langmuir adsorption isotherm through Eq. 9[16].

$$\frac{C}{\theta} = 1/K_{ads} + C \tag{9}$$

where C is inhibitor concentration and K_{ads} is equilibrium constant. Figure 10A displays a plot C/θ as the X-axis against C as the Y-axis, resembling the Langmuir adsorption isotherm. A perfect linear plot was produced with $R^2 = 0.99827$ and a slope of about 0.97796. It is customary that ΔG^0_{ads} pertain to K_{ads}. It could be computed by Eq. 10[11]:

$$K_{ads} = 1/55.5 \exp\left(-(\Delta G^0_{ads}/RT)\right) \tag{10}$$

where ΔG_{ads} is defined as the standard free energy of inhibitor adsorption, 55.5 is known as the molar concentration value of water in the solution, R is the gas constant, and T is the absolute temperature. Exploiting this previous equation, the ΔG^0_{ads} of the inhibitor at 298 K was determined and tabulated in Table 4. When the

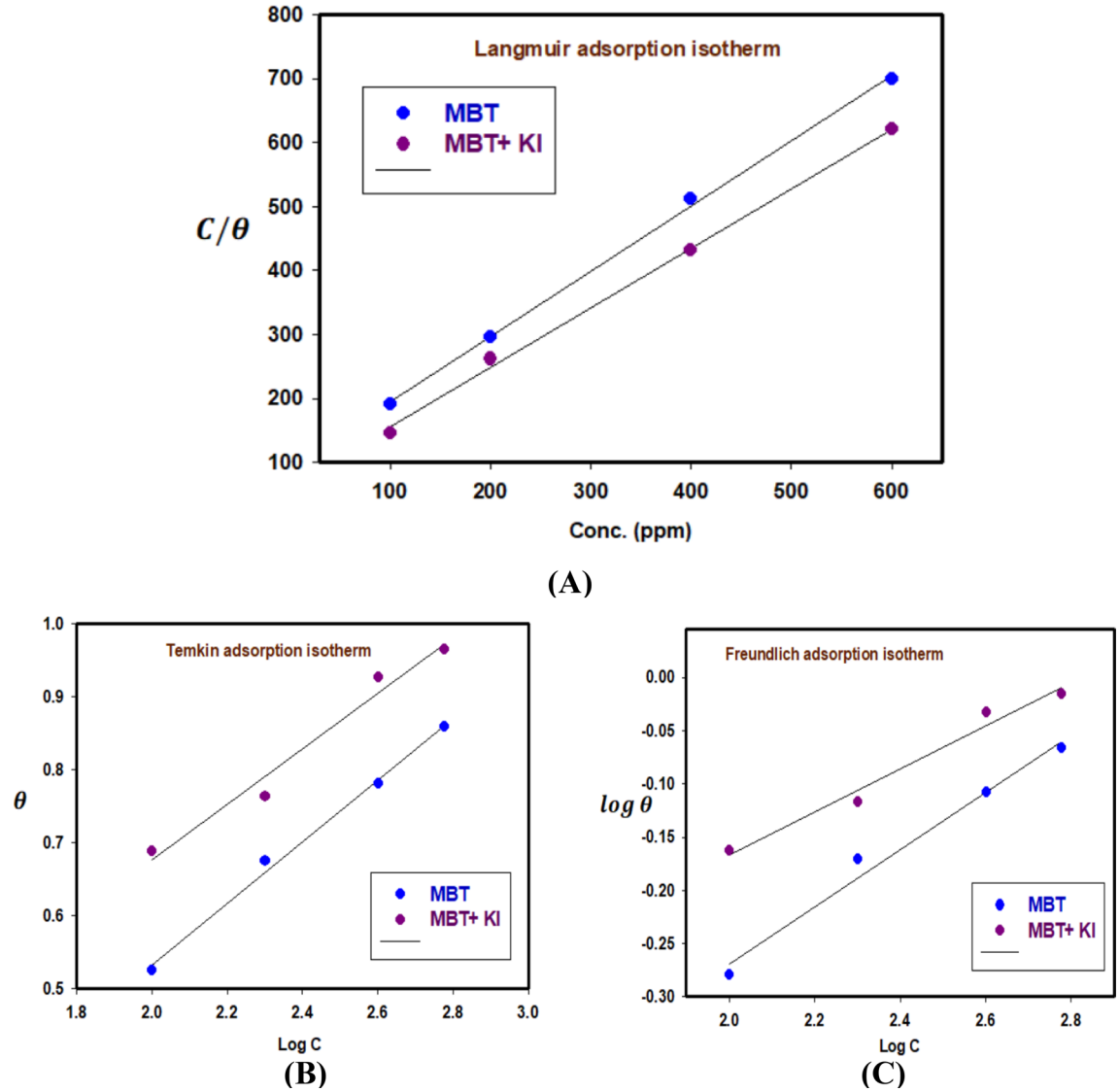

Figure 10. Adsorption isotherm plot from EIS for 304 SS in 1 M HCl in the absence and presence of concentrations of inhibitor at 298 K (MBT and MBT + KI).

Isotherm	Investigated inhibitors	R^2	Slope	K_{ads}	ΔG_{ads} kJ mol^{-1}
Langmuir	MBT	0.99875	1.02160	0.01082	− 21.1644
	MBT + KI	0.99780	0.93432	0.01631	− 20.1486
Temkin	MBT	0.99488	0.42005	1.84645	− 7.02259
	MBT + KI	0.97412	0.37984	1.18077	− 3.78739
Freundlich	MBT	0.98276	0.26885	0.09331	− 9.21462
	MBT + KI	0.97836	0.20107	0.24528	− 8.55157

Table 4. Adsorption parameters for 304 SS in 1 M HCl in the absence and presence of concentrations of inhibitor at 298 K (MBT and MBT + KI).

values of ΔG^0_{ads} are around − 20 kJ mol^{-1} or lower, the adsorption is due to the electrostatic interaction between the charged molecules of the inhibitors and the charged electrode (physic-sorption). Meanwhile, those more negative than − 40 kJ mol^{-1} reveal the charge transfer from the inhibitor to the surface of the metal to form a coordination bond (chemisorption)[21]. The type of observed adsorption (physisorption and chemisorption) is due to that the inhibitor includes more various chemical compounds that can be chemically adsorbed and the others can be physically adsorbed. In this current work, the obtained negative values of ΔG^0_{ads} (less negative than − 20 kJ mol^{-1}) show that the adsorption process of the developed inhibitors on 304 SS in HCl solution is spontaneous and the adsorption technique of the studied inhibitors follows the physic-sorption.

Temkin adsorption isotherm
According to Eq. 11[34], the extent of surface covering is related to the inhibitor concentration and the adsorption equilibrium constant K_{ads}.

$$\exp^{(-2a\theta)} = K_{ads} \times C \tag{11}$$

where a is an attractive parameter and K is the adsorption constant. From Fig. 10B linear plots are obtained, which affirms that the adsorption obeys the Temkin adsorption isotherm. Adsorption parameters obtained from this Figure are shown in Table 4.

Freundlich adsorption isotherm
According to the Freundlich isotherm, θ is related to the inhibitor concentration C using Eq. 12[35].

$$\log\theta = \log K_{ads} + n\log C \tag{12}$$

where n is the empirical constant, and the other constants have the same meaning. Figure 10C shows straight lines relation of log θ against log C with slope n and intercept log K_{ads}. The deduced adsorption parameters K_{ads}, n, and ΔG^0_{ads} are shown in Table 4. The adsorption process was studied using Langmuir, Freundlich, and Temkin isotherms. The adsorption studies indicated that the experimental data satisfied the Langmuir Freundlich and Temkin adsorption isotherms with good linearity. The chosen criteria of the best-fit isotherm are based on the higher correlation coefficient, R^2. The higher value of K indicates that the inhibitor is strongly adsorbed on the 304 SS surface. From Table 4, and Fig. 10A, the fitting was obtained by Langmuir adsorption isotherm with high correlation coefficients (R) as well as with the other two models Temkin–Freundlich isotherm. As shown in Table 4, MBT and MBT + KI ΔG_{ads} values were negative (− 21.1644 and − 20.1486 kJ/mol, respectively), which indicates that their adsorption onto 304 SS surface was a spontaneous process that occurred through physic-sorption (physisorption). Many researchers apply adsorption isotherm to understand the mechanism of adsorption[36]. It is evident from the outcomes that linear R^2 was ~ 0.99827, implying that the adsorption mechanism of MBT and MBT + KI molecules onto 304 SS surface obeyed Langmuir's isotherm.

Chemical kinetics of corrosion inhibiting

The integral method of analysis was used to examine the first-order kinetics. Equation 13 [37] gives this:

$$-\log(\Delta W) = \frac{K_1 t}{2.303} \tag{13}$$

where ΔW is weight in (g), k_1 is the rate constant in (Day^{-1}), and t is the immersion in (Day). In addition, the $t_{0.5}$ first-order reaction is given according to Eq. 14[3]:

$$t_{0.5} = \frac{0.693}{K_1} \tag{14}$$

Figure 11 shows − log (ΔW) against time in (Day) in the absence and presence of different concentrations of MBT and MBT + KI at 298 K. The rate constant and half-life parameters are tabulated in Table 5. The results revealed that the rate constants (K_1) of 304 SS in the presence of MBT or MBT + KI are higher than the rate constant of the blank solution (1 M HCl), while the half-life of 304 SS in the presence of MBT or MBT + KI were less than the half-life obtained for 1 M HCl solution. Based on the results of losing weight over time, the corrosion

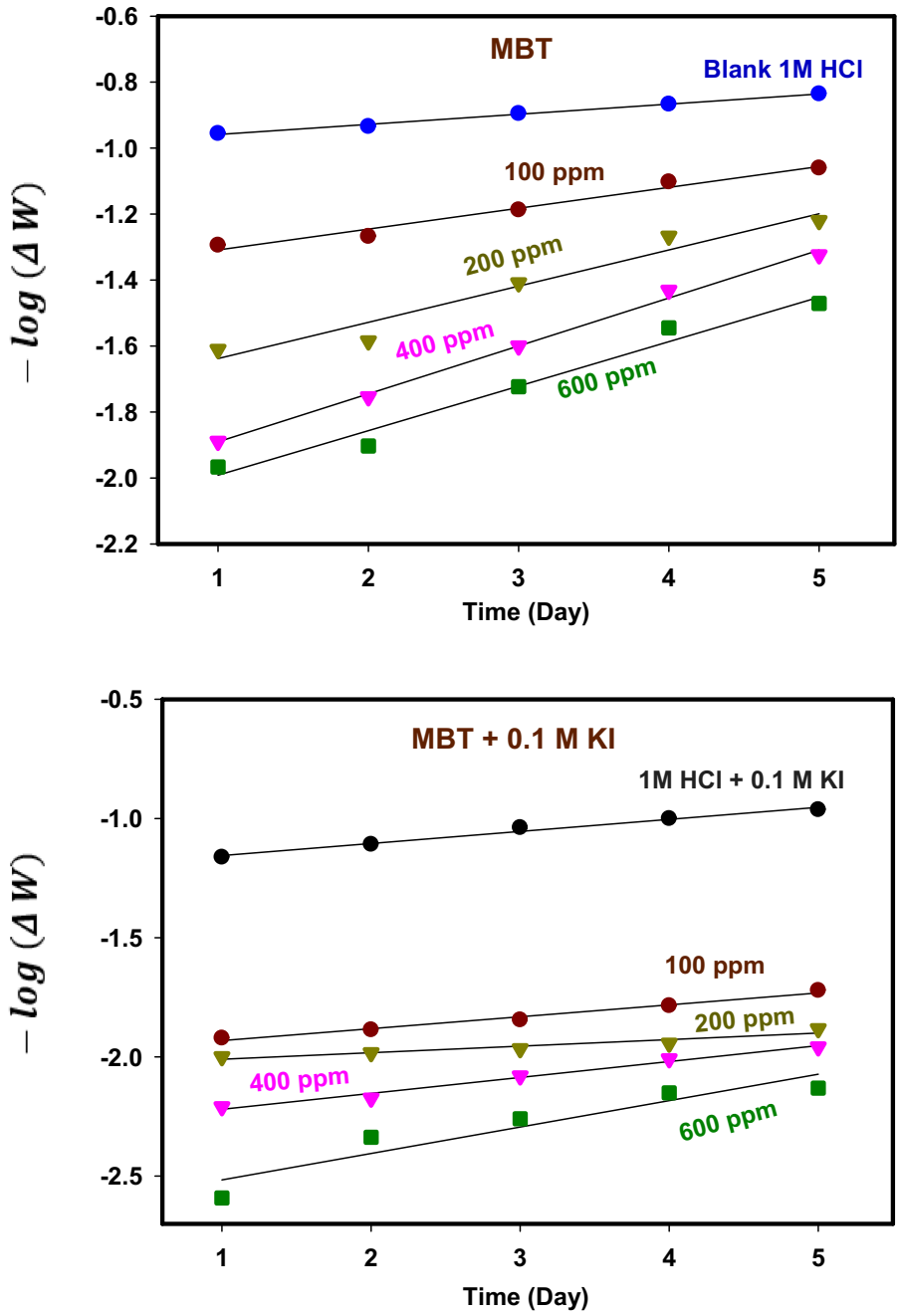

Figure 11. Chemical kinetic plot for 304 SS in 1 M HCl in MBT and MBT + KI at 298 K.

rates and half-life for 304 SS dissolution were somewhat inhibited. These MBTs are thought to be effective inhibitors because they can reduce the amount of time it takes for metals to become corrosion products[38]. The high value of R^2 fitted well with the first-order kinetics conformity with reports of Ijuo et al.[39].

Synergistic impact of KI on effectiveness inhibition

Because halide ions have a stronger propensity to be adsorbed on the surface in interaction with cations by chemisorption[26], it is possible to explain the synergistic inhibition by the combination of MBT and I^- for corrosion 304 SS in 1 M HCl. Inhibition synergism is made by increased surface coverage by electrostatic interaction with protonated Schiff base. Steel anodic and cathodic reactions are polarized by I^- throughout a broad potential range. It becomes clear that covalent bonding to the metal must be involved and that the effects of I^- are not solely due to electrostatic forces. Electron pair bonding is rendered feasible by the huge size and simple polarizability of I^-. Adsorption of the halide ions on the metal surface is followed by the inhibitor being pulled into the double layer by the halide ion, resulting in the formation of ion pairs right on the surface[12]. The synergy between MBT and negatively charged I is interpreted as the cause of the efficiency increase. Studying the key component of the

Systems	Conc. (ppm)	K_1 Day^{-1}	$t_{0.5}$ Day	R^2
Blank 1M HCl	0.0	0.07082	9.7854	0.99409
1M HCl + 0.1M KI	0.0	0.11674	5.9363	0.98358
MBT	100	0.14567	4.7573	0.97503
	200	0.25286	2.7406	0.95108
	400	0.33464	2.0708	0.99608
	600	0.31065	2.2308	0.97384
MBT + 0.1M KI	100	0.11515	6.0182	0.98321
	200	0.16319	4.2465	0.90664
	400	0.15368	4.5094	0.98418
	600	0.25532	2.7142	0.88471

Table 5. Chemical kinetic parameters for 304 SS in 1 M HCl in MBT and MBT + KI at 298 K.

synergistic impact (S) parameter is required to further explore the contribution of I^- to the enhancement of the adsorption mechanism. The following Eq. 15[40] is used to compute the synergism parameter (SI).

$$S_I = \frac{1 - I_{1+2}}{1 - I'_{1,2}} \tag{15}$$

Herein, $(I_{1+2}) = I_1 + I_2$; I_1 = efficiency of halide ions; I_2 = efficiency of used inhibitors, and $(I'_{1,2})$ = efficiency for a mixture of used inhibitors and iodide ions. S values larger than one indicate a synergistic impact whilst, S values less than one indicate an antagonistic action that may result in competing adsorption. Applying the final equation to the efficacies of the experimental methods utilized, such as the gravimetric method, PDP, and EIS technique, this factor was evaluated. The obtained synergism parameter is listed in Table 6. In contrast to systems inhibited using MBT alone, EIS data demonstrate that MBT + KI systems provided the highest value of inhibition efficacy. The interaction between KI and MBT inhibitors has been confirmed by a synergy parameter derived from the EIS data. It is believed that the stability of negative iodide ions and MBT enhances the surface area covered and, as a result, the efficiency value. This demonstrates the synergistic nature of the improved inhibitory efficacy brought about by the addition of iodide ions to MBT[41].

Theoretical studies of MBT inhibitor

The examined inhibitor's optimized molecular structure, together with the associated highest occupied frontier molecular orbital (HOMO), and lowest unoccupied frontier molecular orbital (LUMO), are given in (Figs. 12, 13). The HOMO and LUMO energies are correlated with percent inhibition efficiencies. The percent inhibition efficiencies increase if the molecules have higher HOMO energies and lower LUMO energies[24]. The percent inhibition efficiency increased with a decrease in energy gap (ΔE). The values for E_{HOMO}, E_{LUMO}, and ΔE show that MBH has a somewhat greater ability to act as a corrosion inhibitor. To gain a better understanding of how inhibitor molecules interact with metal surfaces, the present study discusses several additional parameters, including

Conc. (ppm)	S_I (Wt Loss method)	S_I (PDP method)	S_I (EIS method)
100	0.7431	0.8041	1.6642
200	0.9026	1.0875	1.6937
400	0.9798	1.4802	1.5088
600	1.0397	2.7247	1.5294

Table 6. Synergism parameter (S_I) for concentrations of MBT on 304 SS in combination with 0.1 M KI.

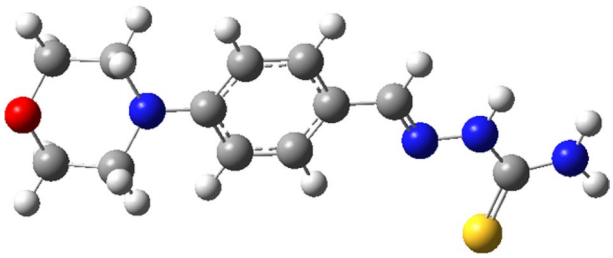

Figure 12. Optimized structure of inhibitor (MBT).

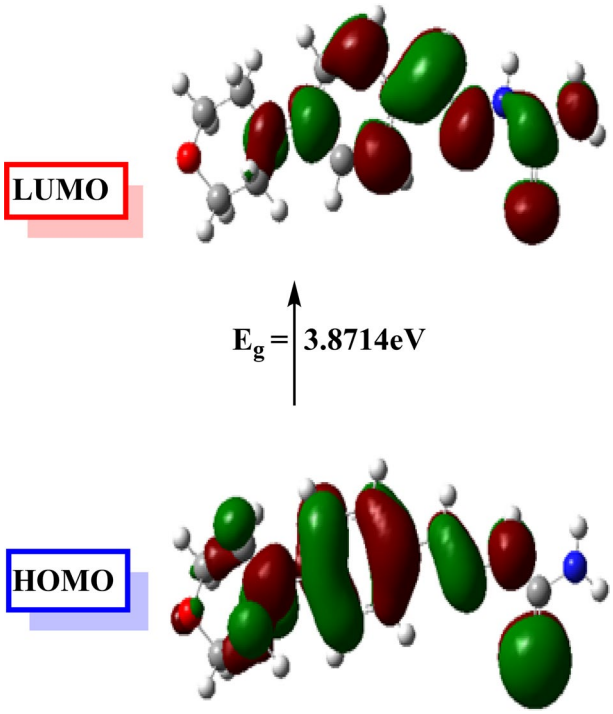

Figure 13. MO and their energies for MBT inhibitor.

global hardness (η), global softness (σ), electronegativity (*X*), chemical potential (u), global electrophilicity (ω), fraction of electron transfer (ΔN) and energy associated with a backing donation (E_{b-d}), Table 7. Furthermore, the relationships used in all of these calculations are presented previously in our publications[24,42]. In general, an inhibitor with a lower global hardness value and a greater softness value corresponds to high chemical reactivity and demonstrates high inhibitory efficiency[25]. Additionally, all of the Schiff base compounds' chemical potential values are negative, as shown in Table 7, indicating that the compounds are stable. Additionally, the MBT inhibitor's high potential value (− 3.4377 eV) and low electrophilicity value (3.4377) favor its nucleophilic behavior[43], this outcome is consistent with the HOMO and LUMO energy values[44]. Fraction of electron transfer (ΔN), this quantity is commonly used to describe a molecule's ability to accept or transfer electrons to or from a metal[44]. If ΔN is more than zero, the inhibitor can donate its electron to the metal, and if ΔN is less than zero, the opposite happens[45]. Thus, the positive values of ΔN for the inhibitor studied imply that the electron donation is from the inhibitor to the metal surface. The negative sign of E_{b-d} suggests that metal-to-inhibitor back donation is energetically beneficial. Back donation and donation methods improve inhibitor adsorption on the iron surface. These findings correspond with the experimental inhibition efficiency.

Parameters	MBH
Total energy, (Hartree)	− 1159.2506
Dipole moment, (Debye)	6.5671
Chemical potential u, (eV)	− 3.4377
Electronegativity *X*, (eV)	3.4377
E_{HOMO}, (eV)	− 5.3734
E_{LUMO}, (eV)	− 1.5020
ΔE, (eV)	3.8714
η, (eV)	1.9357
σ, (eV^{-1})	0.5166
ΔN	0.9201
ω	3.0525
E_{b-d} (eV)	− 0.4839

Table 7. Quantum chemical parameters calculated for CMBAH inhibitor.

Molecular electrostatic potential (MEP)

The molecular electrostatic potential is used to predict the reactivity of inhibitor molecules and the overall charge distribution[46]. As can be seen in Fig. 14, the B3LYP with the basis set 6-31G optimized results were used to create the MEP map of the compound MBT. Colors are used to denote the various MEP surface zones. Indeed, the zone from red to green is favorable for electrophilic attacks. While the zone from green to blue can be attacked by nucleophiles, the green zone represents zero potential.

Biological activity

The newly synthesized Schiff base ligand (MBT) were investigated for their inhibitory effects on the growth of *Bacillus cereus* (G +ve), *E. coli* (G −ve), *Micrococcus luteus* (G +ve), *Pseudomonas aeruginosa* (G −ve), *Serratia marcescens* (G-ve), *Staphylococcus aureus* (G +ve) bacteria and *Aspergillus flavus*, *candida albicans*, *Fusarium oxysporum*, *Geotrichum candidum*, *Scopulariopsis brevicaulis* and *Trichophyton rubrum* fungi. The antimicrobial activity was tested by using the disc diffusion method; the clear zone of inhibition around each disk was measured (in mm) and compared to the known sensitive drugs: chloramphenicol (CHL) as an antibacterial drug and clotrimazole (CLO) as an antifungal drug. The antibacterial and antifungal activities of the prepared MBT are reported in Table 8. The findings suggest that the MBT exhibits greater activity against *Aspergillus flavus*, while the MBT exhibits no activity against the tested bacteria under the experimental conditions.

Corrosion inhibition mechanism

It is necessary to provide an adsorption mechanism to clarify the mechanism of inhibition of the examined molecules during the creation of a protective layer on the metal surface. The inhibitory molecules adsorb on the metal surface due to their strong electrical characteristics, according to the primary findings of the studies and theoretical approaches. Due to chemical and physical adsorption, the generated layers' protective performance has also been demonstrated. It is typically believed that the corrosion process of steel can take place in the unhindered HCl solution in the following ways:

$$Fe + Cl^{-} \leftrightarrow (FeCl)_{ads} + e^{-} \tag{16}$$

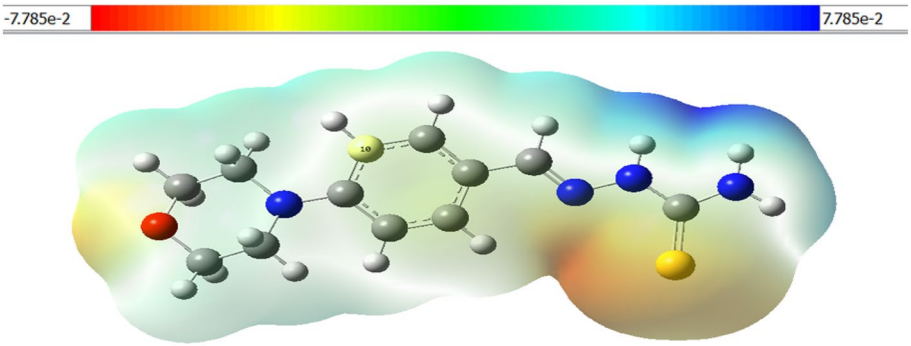

Figure 14. Molecular electrostatic potential (MEP) surface and counterplots for MBT inhibitor.

Bacteria	Compound	
	MBT	CHL
Bacillus cereus (G +ve)	0	22
E. coli (G −ve)	0	20
Micrococcus luteus (G +ve)	0	20
Pseudomonas aeruginosa (G −ve)	0	18
Serratia marcescens (G −ve)	0	20
Staphylococcus aureus (G +ve)	0	18
Fungi	**Compound**	
	MBT	**CLO**
Aspergillus flavus	16	24
Candida albicans	0	22
Fusarium oxysporum	0	18
Geotrichum candidum	0	28
Scopulariopsis brevicaulis	13	22
Trichophyton rubrum	14	42

Table 8. Antibacterial and antifungal activity (inhibition zone in mm) of chemical compounds.

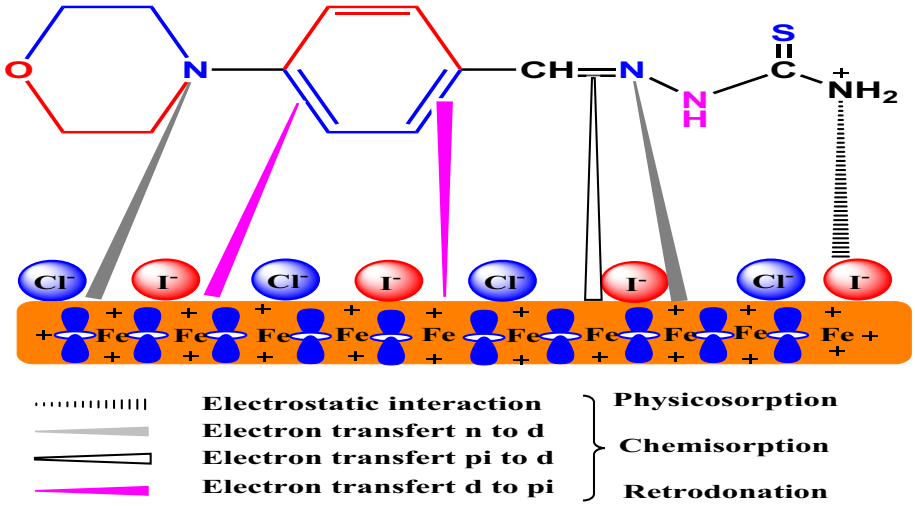

Figure 15. Inhibition mechanism of MBT adsorption on 304 SS.

$$(FeCl)_{ads} \leftrightarrow \left(FeCl^{+}\right) + e^{-} \tag{17}$$

$$\left(FeCl^{+}\right) \leftrightarrow Fe^{2+} + Cl^{-} \tag{18}$$

It observed that the dissolution of the steel in acid has positively charged. The inhibitor compounds typically become protonated when they are present in an acidic environment. In our situation, the protonated form of MBT is expressed as follows when considering the adsorption process:

$$MBT + H^{+} \leftrightarrow [MBT + H]^{+} \tag{19}$$

Due to I^{-} large ionic radius and high hydrophobicity, they participated in the adsorption process onto the steel surface, through a synergetic effect that caused corrosion inhibition. Then under the synergistic effect of MBT + KI, a self-assembled [Fe(0) Fe(II) I^{-}MBT] film can be formed (Fig. 15). The enhanced efficacy of inhibitors in the presence of I^{-} is thus explained by a greater likelihood of donor–acceptor interactions. MBT seems to be a great inhibitor in 1 M HCl, and its potential was enhanced by KI since it achieved 96.57%.

Conclusion

The research summary is based on several significant discoveries, including the following, which are all based on the outcomes of the experiments used:

- MBT is a mixed-type inhibitor according to potentiodynamic polarization data because it prevents the corrosion of 304 SS in acid solution.
- The inhibition efficiency increases with an increase in the concentration of inhibitor.
- The interpretation of the improvement in efficiency is attributed to the synergy between MBT and negatively charged iodide ions. A cooperative effect of iodide ions with MBT is an occurrence.
- The addition of iodide ions to MBT enhanced the inhibition efficiency due to the synergistic effect.
- Adsorption of MBT alone and in mixing with iodide ions on the surface of steel were found to strongly fit Langmuir's adsorption isotherm.
- The thermodynamic parameters calculated from the adsorption isotherms showed that physisorption is involved in the inhibition process.
- DFT findings correspond with the experimental inhibition efficiency.
- MBT exhibits greater activity against *Aspergillus flavus*, while the MBT exhibits no activity against the tested bacteria under the experimental conditions.
- Furthermore, quantum chemical calculations were employed to correlate the experimentally determined inhibitory efficiency.

Data availability

All data generated or analyzed during this study are included in this published article and its supplementary information files.

Received: 10 July 2023; Accepted: 29 December 2023
Published online: 04 January 2024

References

1. Verma, C., Olasunkanmi, L. O., Ebenso, E. E., Quraishi, M. A. & Obot, I. B. Adsorption behavior of glucosamine-based, pyrimidine-fused heterocycles as green corrosion inhibitors for mild steel: Experimental and theoretical studies. *J. Phys. Chem. C* **120**, 11598–11611 (2016).
2. Obot, I. & Edouk, U. M. Benzimidazole: Small planar molecule with diverse anti-corrosion potentials. *J. Mol. Liq.* **246**, 66–90 (2017).
3. Gaber, G. A. Corrosion behavior of Fe-35Ni-22Cr and Fe-17Ni-17Cr alloys in acid pickling solutions. *Egypt. J. Chem.* **63**, 3823–3827 (2020).
4. Abd-Elaal, A. A., Elbasiony, N., Shaban, S. M. & Zaki, E. Studying the corrosion inhibition of some prepared nonionic surfactants based on 3-(4-hydroxyphenyl) propanoic acid and estimating the influence of silver nanoparticles on the surface parameters. *J. Mol. Liq.* **249**, 304–317 (2018).
5. Soliman, S., Metwally, M., Selim, S., Bedair, M. & Abbas, M. A. Corrosion inhibition and adsorption behavior of new Schiff base surfactant on steel in acidic environment: Experimental and theoretical studies. *J. Ind. Eng. Chem.* **20**, 4311–4320 (2014).
6. Bedair, M., El-Sabbah, M., Fouda, A. & Elaryian, H. Synthesis, electrochemical and quantum chemical studies of some prepared surfactants based on azodye and Schiff base as corrosion inhibitors for steel in acid medium. *Corros. Sci.* **128**, 54–72 (2017).
7. El-Rehim, S. A., Deyab, M., Hassan, H. & El-Moneim, A. A. Corrosion and corrosion inhibition of aluminum alloys A5052 and A5754 in sulfuric acid solutions by some inorganic inhibitors. *Z. Phys. Chem.* **231**, 1141–1157 (2017).
8. Heakal, F.E.-T., Osman, M., Deyab, M. & Elkholy, A. Electrochemical and quantum chemical studies on the corrosion inhibition potential of camellia sinensis leaves extract for carbon steel in produced water. *Z. Phys. Chem.* **232**, 13–35 (2017).
9. Gaber, G. A., Hosny, S. & Mohamed, L. Z. Experimental and theoretical studies of 2-cyano-N-(4-morpholinobenzyldine) acetohydrazide as corrosion inhibitor for galvanized steel and 304 stainless steel in 1M H_2SO_4 solution. *Int. J. Electrochem. Sci.* **16**, 211214 (2021).
10. Alahiane, M. *et al.* Corrosion inhibition of SS 316L by organic compounds: Experimental, molecular dynamics, and conceptualization of molecules–surface bonding in H_2SO_4 solution. *Appl. Surf. Sci.* **612**, 155755 (2023).
11. Taha, R. H., Gaber, G. A., Mohamed, L. Z. & Ghanem, W. A. Corrosion inhibition of two schiff base complexes on the mild steel in 1M HCl solution. *Egypt. J. Chem.* **62**, 367–381 (2019).
12. Shaju, K., Thomas, K. J., Raphael, V. P. & Paul, A. Synergistic effect of KI on corrosion inhibition of mild steel by polynuclear Schiff base in sulphuric acid. *Int. Sch. Res. Not.* **2012** (2012).
13. Ahmed, S. K., Ali, W. B. & Khadom, A. A. Synthesis and characterization of new triazole derivatives as corrosion inhibitors of carbon steel in acidic medium. *J. Bio-and Tribo-Corros.* **5**, 15 (2019).
14. Tok, F., Kaya Tilki, E., Dikmen, M. & Kaymakçioğlu, B. Synthesis and anticancer activity of new carbohydrazide derivatives bearing furan moiety. *J. Res. Pharm.* **26** (2022).
15. Ani, F. E. *et al.* Crystal, spectroscopic and quantum mechanics studies of Schiff bases derived from 4-nitrocinnamaldehyde. *Sci. Rep.* **11**, 8151 (2021).
16. Ogunyemi, B. T., Oyeneyin, O. E., Esan, O. T. & Adejoro, I. A. Computational modelling and characterisation of phosphole adopted in triphenyl amine photosensitisers for solar cell applications. *Results Chem.* **2**, 100069 (2020).
17. Ramalingam, A. *et al.* Study of a new piperidone as an anti-Alzheimer agent: Molecular docking, electronic and intermolecular interaction investigations by DFT method. *J. King Saud Univ.-Sci.* **33**, 101632 (2021).
18. Ojo, N. D., Krause, R. W. & Obi-Egbedi, N. O. Electronic and nonlinear optical properties of 3-(((2-substituted-4-nitrophenyl) imino) methyl) phenol. *Comput. Theor. Chem.* **1192**, 113050 (2020).
19. Oyeneyin, O. E. DFT and monte carlo simulations on the corrosion inhibitive potentials of some furan-based carbohydrazide derivatives. *Lett. Appl. NanoBioSci* **12**, 1–22 (2023).
20. Gaber, G. A. *et al.* Study of the corrosion-inhibiting activity of the green materials of the Posidonia oceanica leaves' ethanolic extract based on PVP in corrosive media (1 M of HCl). *Green Process. Synth.* **10**, 555–568 (2021).
21. Gaber, G. A., Maamoun, M. A. & Ghanem, W. A. Evaluation of the inhibition efficiency of a green inhibitor on corrosion of Cu-Ni alloys in the marine application. *Key Eng. Mater.* **786**, 174–194 (2018).
22. Abdel-karim, A. M., Shahen, S. & Gaber, G. 4-Aminobenzenesulfonic acid as effective corrosion inhibitor for carbon steel in hydrochloric acid. *Egypt. J. Chem.* **64**, 825–834 (2021).
23. Frisch, M. *et al.* Gaussian 03, revision c. 02; gaussian, inc.: Wallingford, ct, 2004. *Google Scholar There is no corresponding record for this reference* (2013).
24. Hosny, S., Gouda, G. A. & Abu-El-Wafa, S. M. Novel nano copper complexes of a new Schiff base: Green synthesis, a new series of solid Cr (II), Co (II), Cu (II), Pd (II) and Cd (II) chelates, characterization, DFT, DNA, antitumor and molecular docking studies. *Appl. Organomet. Chem.* **36**, e6627 (2022).
25. Hosny, S., Ragab, M. S. & Abd El-Baki, R. F. Synthesis of a new sulfadimidine Schiff base and their nano complexes as potential anti-COVID-19 and anti-cancer activity. *Sci. Rep.* **13**, 1502 (2023).
26. Lgaz, H. *et al.* Evaluating the corrosion inhibition properties of novel 1, 2, 3-triazolyl nucleosides and their synergistic effect with iodide ions against mild steel corrosion in HCl: A combined experimental and computational exploration. *J. Mol. Liq.* **338**, 116522 (2021).
27. Cenoui, M. *et al.* Synergistic influence of molybdate ions with TDMTAA on corrosion inhibition of ordinary steel in cooling water system. *J. Mater. Environ. Sci* **1**, 84–95 (2010).
28. Li, W.-H., He, Q., Zhang, S.-T., Pei, C.-L. & Hou, B.-R. Some new triazole derivatives as inhibitors for mild steel corrosion in acidic medium. *J. Appl. Electrochem.* **38**, 289–295 (2008).
29. Li, X., Deng, S. & Fu, H. Synergism between red tetrazolium and uracil on the corrosion of cold rolled steel in H_2SO_4 solution. *Corros. Sci.* **51**, 1344–1355 (2009).
30. Ahmed, A. S., Ghanem, W. A., Hussein, W. A. & Gaber, G. A. Evaluation of some inorganic anions and organic compounds as corrosion inhibitors of Cu-Zn alloys in H_2SO_4 and HNO_3 solutions. *Arch. Metall. Mater.* **65**, 639–651 (2020).
31. Dheer, N. *et al.* Synergistic inhibition effect of 3-carboxypyridine and potassium iodide on mild steel corrosion in H_2SO_4: Electrochemical and surface analyses.
32. Mata-Davila, J. *et al.* Electrophoretic deposition of chitosan-hydroxyapatite films and their electrochemical behavior in artificial plasma. *Metals* **13**, 1828 (2023).
33. Shibli, S. & Saji, V. Co-inhibition characteristics of sodium tungstate with potassium iodate on mild steel corrosion. *Corros. Sci.* **47**, 2213–2224 (2005).
34. Verma, C. *et al.* Experimental, density functional theory and molecular dynamics supported adsorption behavior of environmental benign imidazolium based ionic liquids on mild steel surface in acidic medium. *J. Mol. Liq.* **273**, 1–15 (2019).
35. Alahiane, M. *et al.* Experimental and theoretical investigations of benzoic acid derivatives as corrosion inhibitors for AISI 316 stainless steel in hydrochloric acid medium: DFT and Monte Carlo simulations on the Fe (110) surface. *RSC Adv.* **10**, 41137–41153 (2020).
36. Khadom, A. A., Yaro, A. S. & Kadhum, A. A. H. Adsorption mechanism of benzotriazole for corrosion inhibition of copper-nickel alloy in hydrochloric acid. *J. Chil. Chem. Soc.* **55**, 150–152 (2010).

37. Okewale, A. & Adesina, O. Kinetics and thermodynamic study of corrosion inhibition of mild steel in 1.5 M HCl medium using cocoa leaf extract as inhibitor. *J. Appl. Sci. Environ. Manag.* **24**, 37–47 (2020).
38. Orubite-Okorosaye, K. & Oforka, N. Corrosion inhibition of zinc on HCl using Nypa fruticans Wurmb extract and 1, 5 diphenyl carbazonen. *J. Appl. Sci. Environ. Manag.* **8**, 56–61 (2004).
39. Ijuo, G., Chahul, H. & Eneji, I. Corrosion inhibition and adsorption behaviour of *Lonchocarpus laxiflorus* extract on mild steel in hydrochloric acid. *Ew. J. Chem. Kine* **1**, 21–30 (2016).
40. Aramaki, K. & Hackerman, N. Inhibition mechanism of medium-sized polymethyleneimine. *J. Electrochem. Soc.* **116**, 568 (1969).
41. Çalışkan, N. & Bilgic, S. Effect of iodide ions on the synergistic inhibition of the corrosion of manganese-14 steel in acidic media. *Appl. Surf. Sci.* **153**, 128–133 (2000).
42. Sastri, V. & Perumareddi, J. Molecular orbital theoretical studies of some organic corrosion inhibitors. *Corrosion* **53**, 617–622 (1997).
43. Obot, I., Kaya, S., Kaya, C. & Tüzün, B. Theoretical evaluation of triazine derivatives as steel corrosion inhibitors: DFT and Monte Carlo simulation approaches. *Res. Chem. Intermed.* **42**, 4963–4983 (2016).
44. Sharma, K. *et al.* Spectroscopic behavior, FMO, NLO and NBO analysis of two novel aryl boronic acid derivatives: Experimental and theoretical insights. *J. Mol. Struct.* **1181**, 474–487 (2019).
45. Singh, R., Kumar, A., Tiwari, R., Rawat, P. & Gupta, V. A combined experimental and quantum chemical (DFT and AIM) study on molecular structure, spectroscopic properties, NBO and multiple interaction analysis in a novel ethyl 4-[2-(carbamoyl) hydrazinylidene]-3, 5-dimethyl-1H-pyrrole-2-carboxylate and its dimer. *J. Mol. Struct.* **1035**, 427–440 (2013).
46. Zobeidi, A. *et al.* Corrosion inhibition of azo compounds derived from Schiff bases on mild steel (XC70) in (HCl, 1 M DMSO) medium: An experimental and theoretical study. *ACS omega* (2023).

Author contributions

S.H. conceptualization, methodology, sofware, data curation, writing—original draft, investigation, validation, writing—review and editing. A.A. and G.A.G writing—original draft, visualization, data curation, writing—review and editing, sofware.

Funding

Open access funding provided by The Science, Technology & Innovation Funding Authority (STDF) in cooperation with The Egyptian Knowledge Bank (EKB).

Competing interests

The authors declare no competing interests.

Additional information

Supplementary Information The online version contains supplementary material available at https://doi.org/10.1038/s41598-023-51044-w.

Correspondence and requests for materials should be addressed to G.A.G.